Composites: Part B 60 (2014) 479–484

Contents lists available at ScienceDirect

Composites: Part B

journal homepage: www.elsevier.com/locate/compositesb

Pyroshock testing on graphene based EPDM nanocomposites

L. Valentini [a,*], A. Bolognini [b], A. Alvino [c], S. Bittolo Bon [a], M. Martin-Gallego [d], M.A. Lopez-Manchado [d]

[a] Dipartimento di Ingegneria Civile e Ambientale, Università di Perugia, UdR INSTM, Strada di Pentima 4, 05100 Terni, Italy
[b] Dipartimento di Fisica e Laboratorio SERMS, Università degli Studi di Perugia, Strada di Pentima 4, 05100 Terni, Italy
[c] SERMS srl, Strada di Pentima 4, 05100 Terni, Italy
[d] Instituto de Ciencia y Tecnología de Polímeros, ICTP-CSIC, Juan de la Cierva 3, 28006 Madrid, Spain

ARTICLE INFO

Article history:
Received 21 October 2013
Received in revised form 9 December 2013
Accepted 12 December 2013
Available online 27 December 2013

Keywords:
B. Mechanical properties
B. Impact behavior
D. Thermal analysis
B. Hardness

ABSTRACT

Ethylene–propylene–diene terpolymer rubber (EPDM) and graphene nanoplatelets (GNPs) nanocomposites were prepared via a vulcanization process. The mechanical and thermal properties of the nanocomposites were studied. Curing studies demonstrated the increase in maximum torque for the GNP loaded EPDM compounds compared to carbon black loaded EPDM. A high magnitude and a high frequency transient loading, a pyroshock event, was applied to the prepared samples. The acceleration time history measured in the impact excitation test and a simplified analysis model based on the frequency response analysis, were established for evaluating the shock response of the nanocomposites. Experimental results indicated that the interfacial interaction between GNPs and EPDM matrix results in enhancements in damping property. This experimental approach can be used to test the potential utilization of such polymer nanocomposites to be used for space or military components subjected to high-frequency, high-magnitude shock pulses.

1. Introduction

Pyroshock (also called pyrotechnic shock) testing [1–4] is designed to simulate the high-frequency, high-magnitude shock pulse that a product may experience as the result of an explosive event such as the separation of the booster rockets on the space shuttle or an explosive impact on a military structural components.

In aerospace missions pyroshocks occur due to controlled explosions of ordnance devices enabling the functionality of space modules. These shocks result from deployment mechanisms or opening solar sails and can cause failures of electronic devices and structures. Components made of composite materials are of crucial importance for assuring the reliability of aero-space modules and pyroshock tests for the completion of strict requirements have to be met. Consequently it is significant to predict the pyroshock responses on composite materials. The pyroshock prediction is still a complex prediction but one of the most challenging issue in composite science and technology.

The weight saving offered by structural composites make them highly attractive not only to the military, but also to the aerospace and automotive industries. Failures in these structures are mainly attributed to the dynamic loading conditions such as fatigue and vibrations.

High vibration levels often generate excessive noise and leads to cyclic fatigue damage. Polymer damping materials have long been used to reduce vibration levels [5–9]. The vibration isolation property of polymer materials depends significantly on environmental conditions such as temperature, vibration frequency, dynamic load, etc.

These existing damping materials have offered improved damping performance for structural components and systems. But there is a need to develop advanced materials for damping applications, that can overcome these limitations. Recent researches efforts in this direction have been much focused on the development of polymer damping materials based on nanocomposites in which nanotubes, nanofibers or nanoparticles are embedded in polymer substrates and much promising results have been established [10–12].

The research on rubber nanocomposites can be both fundamental and applied, and has attracted growing attention. Numerous studies have demonstrated that the uniform distribution of nanoscaled filler particles into a rubber matrix, with reasonably good interfacial bonding strength, could lead to a rubber nanocomposite with significantly improved properties [13–20].

Rubber is an important commercial material widely being used not only for automobile and industrial applications but also for space components [21,22]. Since rubber for space application requires good reinforcement at the minimum possible filler loading, incorporation of few percentage of graphene nanoplatelets is a viable alternative to obtain low density high performance composites.

* Corresponding author. Tel.: +39 0744 492924.
E-mail address: luca.valentini@unipg.it (L. Valentini).

1359-8368/$ - see front matter © 2013 Elsevier Ltd. All rights reserved.
http://dx.doi.org/10.1016/j.compositesb.2013.12.022

The mechanical properties of such matrix containing equal amount of graphene nanoplatelets and carbon black was the optimum compared to those containing either graphene nanoplatelets or carbon black [23].

The demand for improving the performance of structural materials makes dynamic analysis an important consideration. In this paper, for the first time to our best knowledge, we report a simplified analysis model based on the frequency and the impact energy for evaluating the shock response of graphene based ethylene–propylene–diene terpolymer rubber (EPDM) nanocomposites.

2. Experimental details

2.1. Materials and sample preparation

Ethylene–propylene diene terpolymer rubber (EPDM) was kindly supplied by Exxon Mobil Chemical under the trade name Vistalon 7500 (ethylene content: 56.0 wt.% and 5-ethylidene-2-norbornene (ENB) content: 5.7 wt.%). Carbon black was kindly supplied by Cabot, S.A. under the trade name Vulcan 3-N330 and a paraffinic oil kindly supplied by Nynas, Nyflex 820 was used as plasticizer. Graphene nanoplatelets were purchased from Cheaptubes® (diameter and thickness of GNPs were assumed from scanning electron microscopy imaging to be 15 μm and 30 nm, respectively).

Rubber compounds were prepared in an open two-roll mill at room temperature. The rotors operated at a speed ratio of 1:1.4. The vulcanization ingredients were added to the elastomer previously to the incorporation of the filler and, finally, sulfur was added. The recipes of the compounds are described in Table 1. The percentage of carbon black was calculated as the ratio between the parts per hundred of EPDM and carbon black (i.e. 48% for EPDM-2 and EPDM-3 and 24% for EPDM-4). The percentage of GNPs was calculated as the ratio between the parts per hundred of EPDM and GNPs (i.e. 5% for EPDM-3 and 2.5% for EPDM-4). The vulcanizing conditions (temperature and time) were previously determined by a Monsanto Moving Die Rheometer MDR 2000E. Rubber compounds were vulcanized at 160 °C in a thermofluid heated press. The vulcanization time of the samples corresponds with optimum cure time t_{90} derived from the curing curves of the MDR 2000E. Specimens were mechanically cut out from the vulcanized plaques.

The thermal stability of the compounds was determined from thermogravimetric analysis (TGA) using a TA Mettler Toledo thermogravimetric analyzer (TGA, model SDTA 851). Thermograms of approximately 10 mg were recorded from 40 °C to 600 °C, at a heating rate of 10 °C/min under a nitrogen flow and then, up to 800 °C in oxygen atmosphere to degrade the carbon material.

Tensile stress–strain properties were measured according to ISO 37-1977 specifications, on an Instron dynamometer (Model 4301), at 25 °C at a crosshead speed of 500 mm min^{-1}. Shore hardness was measured by using a Bareiss Rockwell tester according to ASTM D-2240. In all of the tests, data were used as the average of at least five measurements.

Table 1
Recipes of the rubber compounds (indicated in phr: parts per hundred of rubber).

Ingredient	EPDM-1	EPDM-2	EPDM-3	EPDM-4
EPDM Vistalon 7500	100	100	100	100
Paraffinic oil	80	80	80	80
Zinc oxide	5	5	5	5
Stearic acid	1	1	1	1
TMTD	1.5	1.5	1.5	1.5
Sulfur	3	3	3	3
Carbon black	–	190	190	95
Graphene nanoplatelets	–	–	20	10

The dynamic mechanical properties of the composites were determined with a rheometer at a frequency of 1 Hz and the temperature programs were run from −100 °C to 50 °C at a heating rate of 2 °C/min in a flow of nitrogen.

The morphology of the cross section of the prepared samples was investigated by field emission scanning electron microscopy (FESEM, Zeiss Supra 25). The films surface was observed by FESEM operating at 5.0 kV accelerating voltage without deposition of any conductive coating.

2.2. Pyroshock test

An air gun is clamped at both ends and it is attached to a massive base structure, to impose a fixed-end condition on the beam (Fig. 1). A resonant steel plate was put just in front of the beam and it is used to generate the desired pyroshock test pulse. The fixture is clamped to the top near the end of the barrel. The target is mounted on the steel plate and an accelerometer, used to measure the shock pulse during the test, is fixed to the back side of the resonant plate. The accelerometer used for the testing is manufactured by PCB Piezotronics and designed specifically for pyroshock testing with a range of up to 100,000 g. The resonance of the fixture is excited by an impact produced by a captive cylindrical projectile in the air gun. The mass and the length of the projectile were 1.800 kg ± 0.001 kg and 150.00 mm ± 0.05 mm, respectively. The velocity of the projectile was measured with an optical control mounted at the end of the gun barrel and in proximity of the target (Fig. 1). The impact velocity was varied between 3 m/s and 22 m/s resulting in an impact energy varying from 10 J to 510 J, respectively. For a fixed velocity, three tests were repeated on each sample; the experimental error was estimated below 1%. When the target is struck with a cylindrical mass fired from the air gun beneath it, the transient acceleration response was measured by the accelerometer. The impact loading was applied at the center of the sample by the stricking projectile.

In order to achieve the most reliable data, the following parameters have been used for recording:

Sampling frequency	102,400 Hz
Acquisition time	1.28 s
Measurement mode	Triggered
Pre-trigger	0.1 s
Trigger slope	Up
Trigger level	0.0015 V
Averaging	None

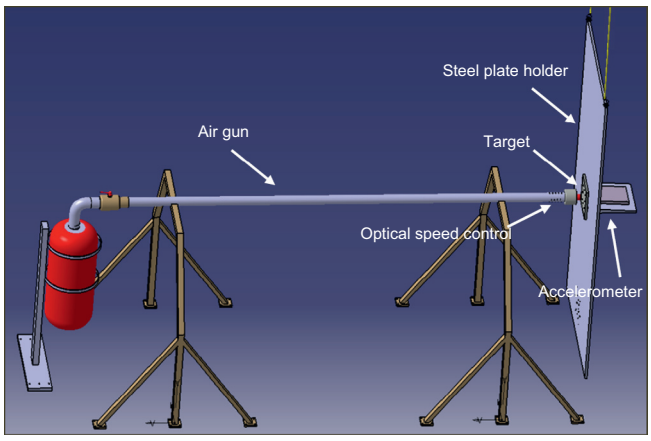

Fig. 1. Scheme of the set-up for pyroshock testing.

3. Results and discussion

The curing characteristics of the composites, torque delta and optimum cure time (t_{90}), analysed at 160 °C on a Monsanto oscillating disc curemeter, are summarized in Table 2. t_{90} hardly varies in presence of the carbon nanoparticles, however, the torque value gradually increases when the carbon filler content in the composites is increased. So, the hybrid composite with both nanoparticles, carbon black and graphene nanoplatelets, shows the higher torque value. Assuming that the torque value derived from curemeter curves, is related to the crosslinking density, the hybrid nanocomposite has a higher number of crosslinks than carbon black nanocomposites. The sample with the highest GNP content shows the highest t_{90} value.

The tensile properties given in terms of the modulus at different strains (50%, 100%, and 300%), the maximum strength and elongation at break are reported in Table 2. As expected, the high filler contents in the composite give rise to an increase of the stiffness of the material which is reflected in an improvement of the strength at low strains and a reduction of the elongation at break. This effect is more marked in the case of the hybrid composites where increments above 300% are obtained. These results are in concordance with the hardness measurements where a gradually increases with the carbon nanoparticles content in the composite is observed. In fact, the hybrid nanocomposite shows the higher hardness values demonstrating its higher stiffness.

The thermal stability of pristine EPDM and its nanocomposites was characterized by thermogravimetric analysis (Fig. 2). EPDM reveals two-stage degradation, the first stage around 330–335 °C involves the degradation of oil, and the second step associated to the thermal degradation of polymer chains occurs at around 480–485 °C. A similar behavior is observed for the nanocomposites. However, in this case, a third step above 600 °C corresponding to the degradation of the carbon nanoparticles under oxygen atmosphere is observed. It is of interest to note that the thermal stability of EPDM is slightly improved in presence of nanoparticles.

Fig. 3 shows the variation tanδ with temperature for EPDM nanocomposites. From Fig. 3, it can be seen that the glass transition temperature of EPDM-2 increased slightly with the incorporation of GNPs. In general, the increase in T_g is attributed to the restriction of the segmental motion of cross-links under loading [24].

Fig. 4 reports the acceleration time history measured in the impact excitation test. The damping of the sample can be qualitatively estimated by the relative variation of the acceleration peak after the impact. It is evident how the damping effect depends on the impact energy and the sample composition. In particular, for low velocity of the projectile and thus low impact energy (velocity ≈ 3 m/s and energy ≈ 10 J), the EPDM-2 sample has a better damping effect with respect to the sample with the highest GNP content (i.e. EPDM-3). The EPDM-4 showed the best damping property at such energy but with a small relative variation of the acceleration after the impact (Fig. 4a).

On the contrary at higher impact energy (velocity ≈ 22 m/s and energy ≈ 500 J) the EPDM-3 sample absorbs the energy much better than the EPDM-2 one (Fig. 4b). At such energy the EPDM-4 sample did not pass the test. In fact, the high acceleration recorded on

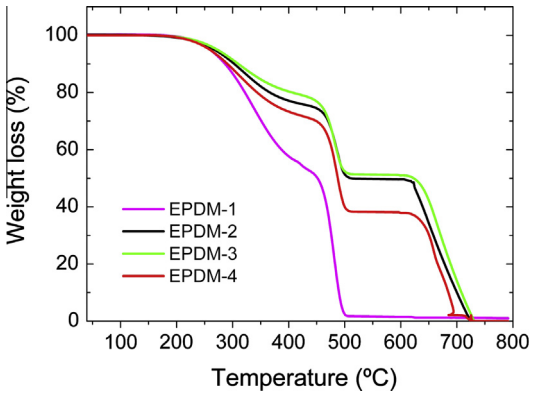

Fig. 2. Thermal degradation of EPDM and its carbon nanocomposites.

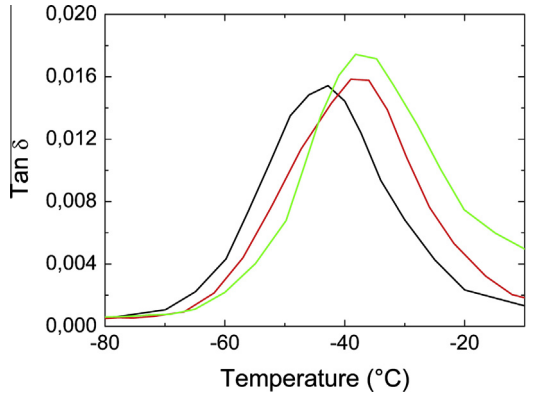

Fig. 3. Dynamic mechanical spectra for EPDM-2 (black), EPDM-4 (red) and EPDM-3 (green) samples. (For interpretation of the references to color in this figure legend, the reader is referred to the web version of this article.)

sample EPDM-4 was due to the failure of the sample that was perforated by the projectile during the impact (see below). Thus the time history on such sample recorded only the impact between the projectile and the steel plate.

Shock Response Spectrum (SRS) represents the description of the shock in terms of the effect on structures when the shock acts as the excitation. In particular the SRS is defined as the absolute value of the maximum of the positive and negative acceleration responses of a mass for a given base input to a damped single degree of freedom (SDOF) as reported in Fig. 5a; the input base displacement is $z(t)$ and the response displacement of the mass is $u(t)$. The damping force (F_c) is proportional to velocity due to the viscous damper with damping constant, c: $F_c = -c(du/dt - dz/dt)$. The critical damping for a SDOF system is $c_c = 2(\mathrm{km})^{1/2}$ with the damping ratio, ζ, equal to $c/c_c = c/2(\mathrm{km})^{1/2}$.

Thus the SRS is related to the damping factor of the samples. Fig. 5 shows the SRS spectra measured in the impact excitation test. The knee frequency is the dominant frequency in a pyroshock SRS, at which the slope for the SRS changes to an approximately horizontal slope or plateau with peaks at the major local structural

Table 2
Vulcanizing characteristics and mechanical properties of the studied materials.

	Torque (dNm)	t_{90} (min)	Strength 50% elong. (MPa)	Strength 100% elongation (MPa)	Strength 300% elongation (MPa)	Max. strength (MPa)	Elong. at break (%)	Hardness shore A
EPDM-1	13.22	26.9	1.6	2.4	4.2	8.3	567	60.5
EPDM-2	29.09	29.4	4.2	7.8	–	11.3	115	86.0
EPDM-3	31.37	33.4	6.8	–	–	9.6	85	90.6
EPDM-4	21.58	27.8	3.6	6.4	–	19.4	283	69.4

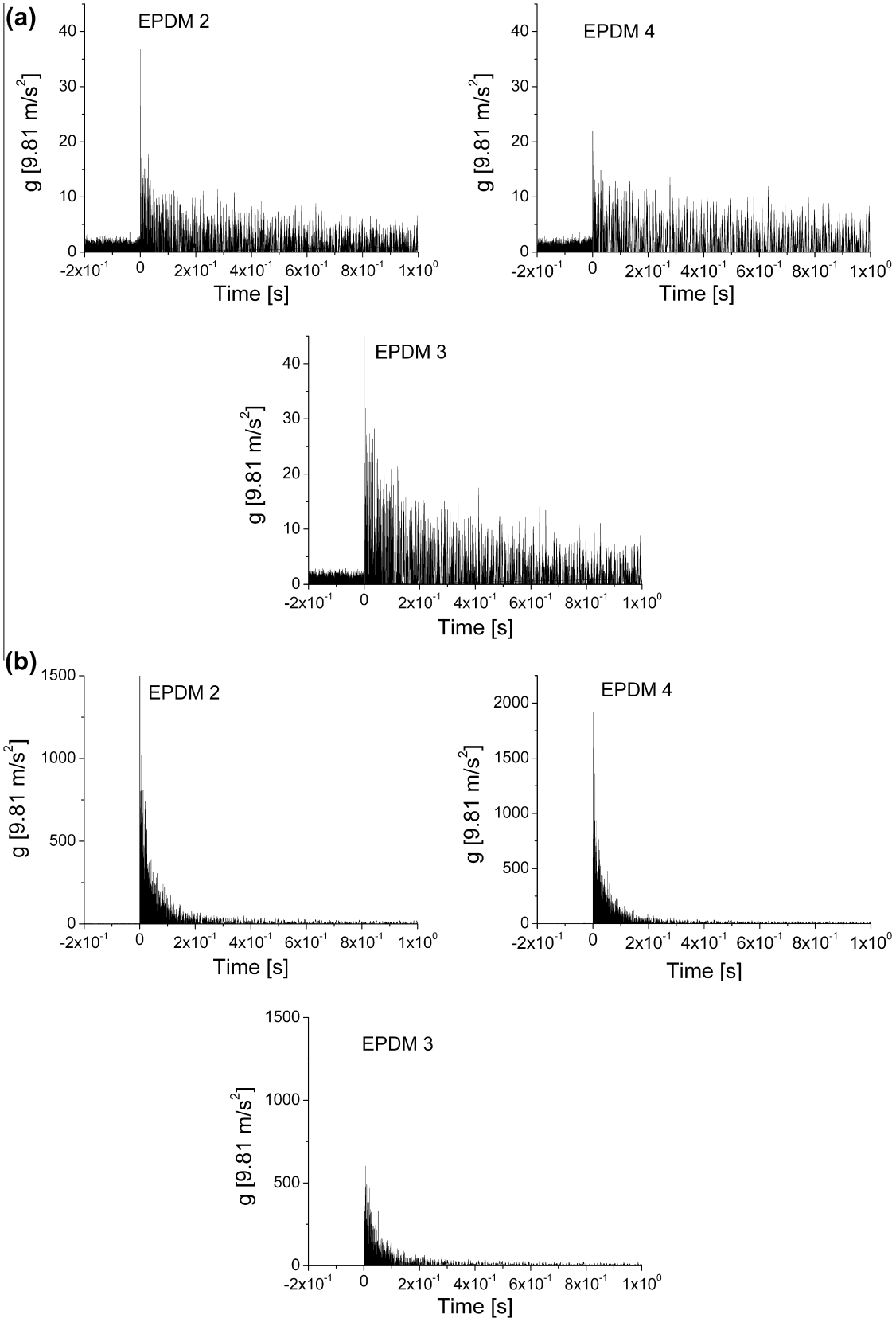

Fig. 4. Positive acceleration time history for the prepared samples during the impact with a velocity of the projectile of (a) 3 m/s and (b) 22 m/s, respectively.

frequencies. The main peak predicted by the analytical model appear to be systematically shifted to higher frequencies for higher impact energy. At low energy (Fig. 5b) the absence of peaks for the EPDM-4 sample indicates a small damping effect for such sample. This results is in agreement with the small variation of the acceleration after the impact reported in Fig. 4a. The EPDM-2

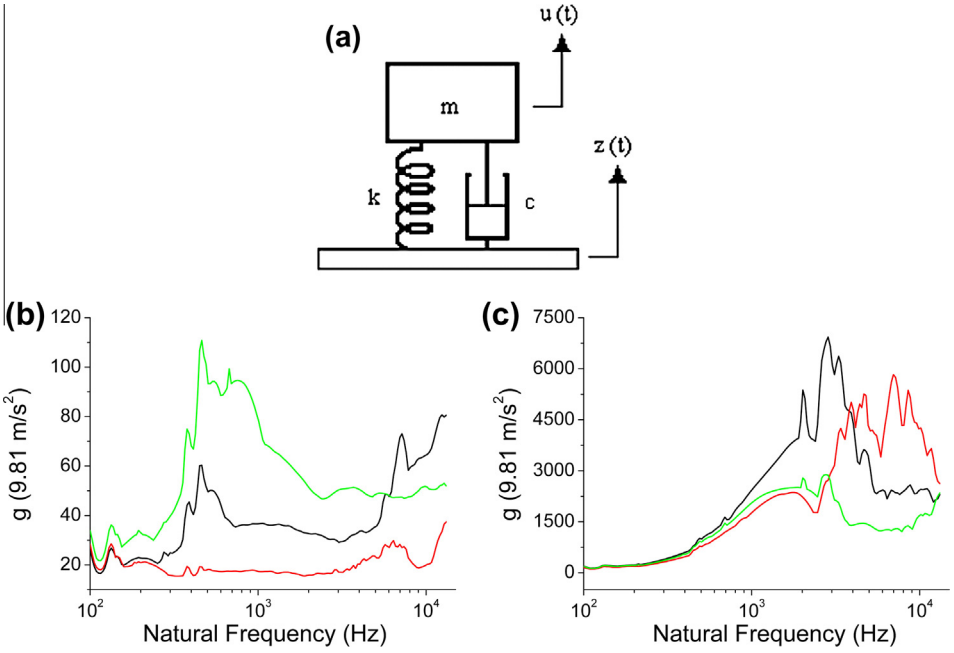

Fig. 5. (a) A SDOF system responding with motion $u(t)$ to base motion $z(t)$. SRS for EPDM-2 (black), EPDM-4 (red) and EPDM-3 (green) samples during the impact with the velocity of the projectile of (b) 3 m/s and (c) 22 m/s, respectively. (For interpretation of the references to color in this figure legend, the reader is referred to the web version of this article.)

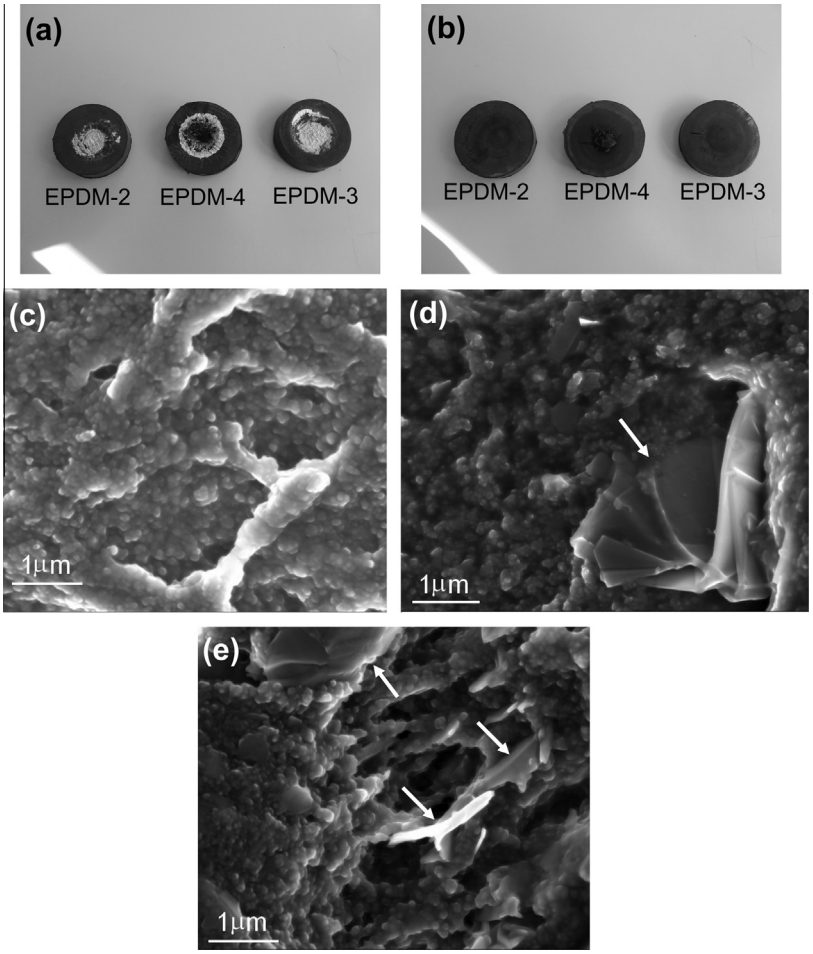

Fig. 6. Photographs of (a) impact side and (b) back side of EPDM-2, EPDM-4 and EPDM-3 samples, respectively. FESEM images of (c) EPDM-2, (d) EPDM-4 and (e) EPDM-3 samples. The arrows in the panels (d and e) serve to indicate the GNPs dispersed into the polymer matrix.

sample shows absorption peak with lower intensity than that observed for the EPDM-3 sample indicating a lower acceleration transferred to the accelerometer after the impact and thus a better performance in terms of damping effect.

The peak for the impact at high energy level (Fig. 5c) shifts to higher frequency values, with a lower intensity for the EPDM-3 sample with respect to the EPDM-2. The peak recorded for the EPDM-4 sample corresponds to vibration frequency of the steel plat due to the failure of the sample (Fig. 6a and b).

From Figs. 4 and 5, the following observations can be made: (a) at low energy impact the carbon black content plays a crucial role under a critical concentration of GNPs (i.e. below 5%); (b) at high energy impact the damping effect of the EPDM nanocomposite with the highest content of GNP is larger than that of carbon black filled EPDM. Such findings could indicate that the GNP slip plays a key role in enhancing damping property at high energy.

These results support the existence of a "stick-slip" motion between polymer matrix and GNP fillers [25]. The damping effect of nanocomposite containing graphene is activated by the impact energy and thus it is larger at high impact energy, which results mainly from the effect of contact area and weak interfacial interaction between EPDM matrix and GNPs (Fig. 6d and e). The large contact area and weak interfacial interaction increase the energy dissipation due to interfacial friction.

According to previous studies [26,27], when the energy is low then the strain is very small; the free volume and the fractional free volume increase with the strain.

However as observed for the EPDM-2 sample, when the impact energy increases and the strain increases further, the damping effect decreases. Wang et al. [28] attributed this effect to the orientation of chain segments and to the occurrence of ordered arrangement of the segments that reduce the damping effect.

Because of the small size of GNPs, the interfacial area between the GNPs and EPDM is extremely large, leading to large frictional force and damping by the deformation. This finding explains the activation of the damping at high impact energy.

4. Conclusions

Ethylene–propylene–diene terpolymer rubber and graphene nanoplatelets nanocomposites were prepared via a vulcanization process. It was observed how such hybrid nanocomposite has a higher number of crosslinks than carbon black nanocomposites. The hybrid nanocomposites showed a higher hardness values demonstrating their higher stiffness. Pyroshock test and analysis are used to extract damping properties of hybrid EPDM nanocomposites. It is observed that increasing the GNP content along with the impact energy causes an increase in the damping properties. The damping ratio of hybrid composites depending on the GNP content and on the impact energy, was rationalized in terms of the stick-slip concept in nanocomposites.

Acknowledgments

Dr. Lucia Di Masso, CEO of SERMS srl, is kindly acknowledged for the utilization of the pyroshock facility.

References

[1] Davie N, Bateman V. Shock and vibration handbook. McGraw-Hill; 1995.
[2] Lai ML, Soom A. Statistical energy analysis for the time-integrated transient response of vibrating systems. Trans Am Soc Mech Eng 1990;112:206–13.
[3] Shi P. Simulation of impact involving an elastic rod. Comput Methods Appl Mech Eng 1998;151(3–4):497–9.
[4] Mao Y, Huang H, Yan Y. Numerical techniques for predicting pyroshock responses of aerospace structures. Adv Mater Res 2010;108–111:1043–8.
[5] Tahan Latibari S, Mehrali M, Mottahedin L, Fereidoon A, Metselaar HSC. Investigation of interfacial damping nanotube-based composite. Compos B Eng 2013;50:354–61.
[6] Kosmatka JB, Liguore SL. Review of methods for analyzing constrained layer damping structures. J Aerosp Eng 1993;6:268–83.
[7] Baz A, Ro J. The concept and performance of active constrained layer damping treatments. J Sound Vib 1994;28:18–21.
[8] Liao WH, Wang KW. On the analysis of viscoelastic materials for active constrained layer damping treatments. J Sound Vib 1997;207:319–34.
[9] Spitas V, Spitas C, Michelis P. Modeling of the elastic damping response of a carbon nanotube–polymer nanocomposite in the stress–strain domain using an elastic energy release approach based on stick-slip. Mech Adv Mater Struct 2013;20(10):791–800.
[10] Buldum A, Lu JP. Atomic scale sliding and rolling of carbon nanotubes. Phys Rev Lett 1999;83:5050–3.
[11] Ru CQ. Effect of van der Waals forces on axial buckling of a double-walled carbon nanotube. J Appl Phys 2000;87(10):7227–31.
[12] Suhr J, Koratkar N, Keblinski P, Ajayan P. Viscoelasticity in carbon nanotube composites. Nat Mater 2005;4:134–7.
[13] Hamed GR. Rubber reinforcement and its classification. Rubber Chem Technol 2007;80:533–44.
[14] Mertz G, Hassouna F, Leclère P, Dahoun A, Toniazzo V, Ruch D. Correlation between (nano)-mechanical and chemical changes occurring during photo-oxidation of filled vulcanised styrene butadiene rubber (SBR). Polym Degrad Stab 2012;97(11):2195–201.
[15] Bashir MA, Shahid M, Alvi RA, Yahya AG. Effect of carbon black on curing behavior, mechanical properties and viscoelastic behavior of natural sponge rubber-based nano-composites. Key Eng Mater 2012;510–511(1):532–9.
[16] Ma J, Xiang P, Mai Y, Zhang L. A novel approach to high performance elastomer by using clay. Macromol Rapid Commun 2004;25:1692–6.
[17] Fu J-F, Chen L-Y, Yang H, Zhong Q-D, Shi L-Y, Deng W, et al. Mechanical properties, chemical and aging resistance of natural rubber filled with nano-Al_2O_3. Polym Compos 2012;33(3):404–11.
[18] Arroyo M, Lopez-Manchado MA, Herrero B. Organo-montmorillonite as substitute of carbon black in natural rubber compounds. Polymer 2003;44:2447–53.
[19] Lopez-Manchado MA, Biagiotti J, Valentini L, Kenny JM. Dynamic mechanical and Raman spectroscopy studies on interaction between single-walled carbon nanotubes and natural rubber. J Appl Polym Sci 2004;92:3394–400.
[20] Hernandez M, Bernal MD, Verdejo R, Ezquerra TA, Lopez-Manchado MA. Overall performance of natural rubber/graphene nanocomposites. Compos Sci Technol 2012;73:40–6.
[21] Rajeev RS, Bhowmick AK, De SK, Bandyopadhyay S. Short melamine fiber filled nitrile rubber composites. J Appl Polym Sci 2003;90(2):544–58.
[22] Narayanan E, Bhagawan SS, John B, Bhaskaran AK. Space quality rubber products: case study with nitrile/butadiene rubber based engine gimbal control system bladder. Plast Rubber Compos Process Appl 1998;27(7):337–40.
[23] Varghese TV, Kumar HA, Anitha S, Ratheesh S, Rajeeev RS, Rao VL. Reinforcement of acrylonitrile butadiene rubber using pristine few layer graphene and its hybrid fillers. Carbon 2013;61:476–86.
[24] Becker O, Varley R, Simon G. Morphology, thermal relaxations and mechanical properties of layered silicate nanocomposites based upon high-functionality epoxy resins. Polymer 2002;43:4365–73.
[25] Zhou X, Shin E, Wang KW, Bakis CE. Interfacial damping characteristics of carbon nanotube-based composites. Compos Sci Technol 2004;64:2425–37.
[26] Wang B, Wang CL, Li SQ, Wang SJ. Investigation of uniaxially drawn polyethylene by positron-annihilation. Phys Status Solidi A 1994;144:263–9.
[27] Wang CL, Mohsen M, Abd-El Salam MH, Ashry A, Ismail A, Ismail H. Positron annihilation spectroscopy in carbon black-silica-styrene butadiene rubber (SBR) composites under deformation. Polym Degrad Stab 2005;87:381–8.
[28] Wang B, Li SQ, Wang SJ. Effects of deformation on the microstructure of PTFE polymer studied by positron-annihilation. J Phys: Condens Matter 1993;5:7515–20.